the effect of the interface layer cannot be neglected, Eq. (3-22) becomes

$$qN_AW_1 = qN_I^*W_{OB} + Q_{rI} + Q_{ss} \quad (3\text{-}26)$$

$$= qN_I^*W_{OB} + Q_{rI} + N_s^*d_s \quad . \quad (3\text{-}27)$$

The parameters used in the present simulation are given in Table 3-2 and almost all the parameters are fixed, since the purpose in this section is to understand the physical background of the space-charge density (N_I) as well as the built-in potential (V_B) obtained from the steady-state HMC method which is described in the former section. The value of ε_{s1} is also assumed to be equal to the value of ε_{s2}.

3-3-3. Reliability of steady-state HMC method

Figure 3.12(a) shows the simulated high-frequency C-V characteristics of a highly resistive amorphous/lowly resistive crystalline heterojunction (with parameters of $g_{max}=10^{16}$ $cm^{-3}eV^{-1}$ and $N_A=10^{15}$ cm^{-3}), and Fig. 3.12(b) shows the W_1^2-V relation obtained from the C-V curve given in Fig. 3.12(a) by using Eq. (3-10). According to the steady-state HMC method [Eq. (3-11)], the values of N_I and V_B can be graphically obtained from the slope and the intercept on the abscissa, respectively. The value of N_I obtained in the reverse-bias region ($-6\ V \leqq V \leqq -1\ V$) is 2.5×10^{15} cm^{-3}. This value is close to N_I^* of 2.0×10^{15} cm^{-3} calculated from Eqs. (3-16) and (3-17) using the parameters given in Table 3-2 ($g_{max}=10^{16}$ $cm^{-3}eV^{-1}$). The value of V_B, which is obtained from the intercept of the straight line drawn in the reverse-bias region ($-6\ V \leqq V \leqq -1\ V$) on the abscissa, is 0.21 V. This value is a little lower than the given value of $V_B^*=0.30$ V, because the additional potential u_{OB}/q is necessary to make the space-charge density constant. Figure 3.13 depicts N_I and V_B as a function of N_I^*. Figure 3.14 shows the dependence of N_I and V_B on N_A. From both figures, N_I represents the midgap-state density well, although N_I is a little larger than the given value of N_I^*.

The simulated high-frequency C-V characteristics, in which

TABLE 3-2. Parameters used for simulating high-frequency C-V characteristics.[a,b]

Amorphous film			
Neutral region	Midgap states	Interface layer	Others
$E_C-E_F^a$=0.73 eV $E_C-E_{OB}^a$=0.97 eV	E_C-E_p=0.85 eV E_W=0.10 eV $g_{max}=10^{16}-10^{17}$ $cm^{-3}eV^{-1}$	$N_S^*=0-10^{18}$ cm^{-3} d_S=0 or 50 Å	V_B^*=0.3 V L=1.2 μm S=0.785 mm^2 $N_A=10^{15}-10^{17}$ cm^{-3}

[a] N_I^* is calculated from Eq. (3-16) using the given g_{max}.
[b] N_I and V_B obtained from the steady-state HMC method correspond to the parameters N_I^* and V_B^* for the simulation, respectively.

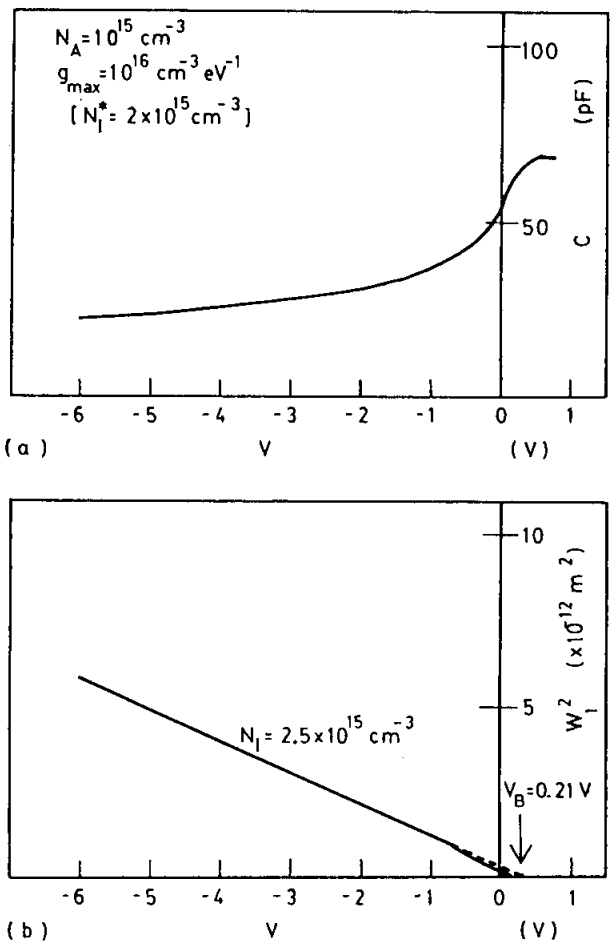

Fig.3.12. Calculated results without interface layer; (a) calculated C-V characteristics and (b) voltage dependence of square of depletion width in crystalline semiconductor. The values of N_I and V_B are obtained from the steady-state HMC method. The solid line is calculated data, and the dashed line is a line extrapolated from high reverse biases.

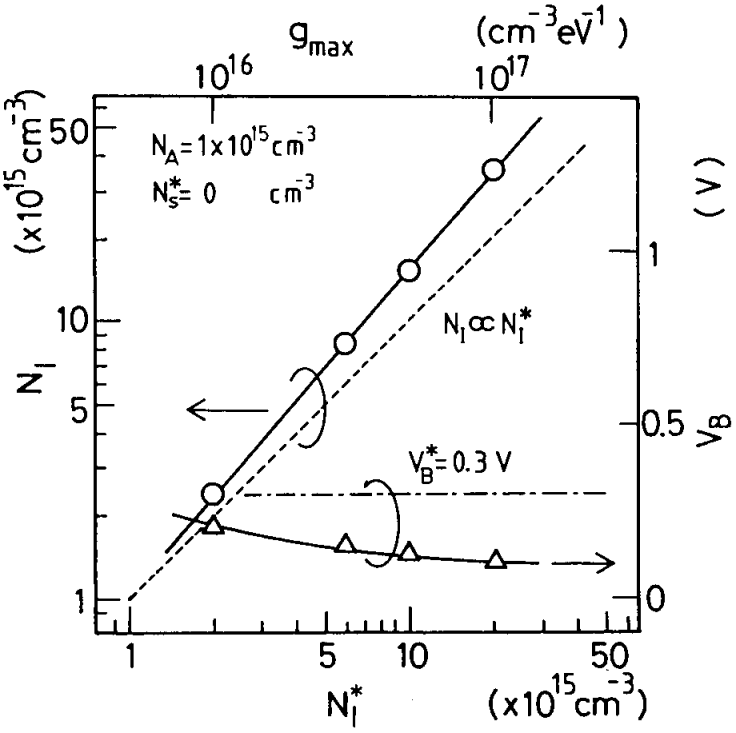

Fig.3.13. Dependencies of N_I and V_B obtained from steady-state HMC method on N_I^* without interface layer. The values of N_I^* and V_B^* are parameters for simulating the high-frequency C-V characteristics.

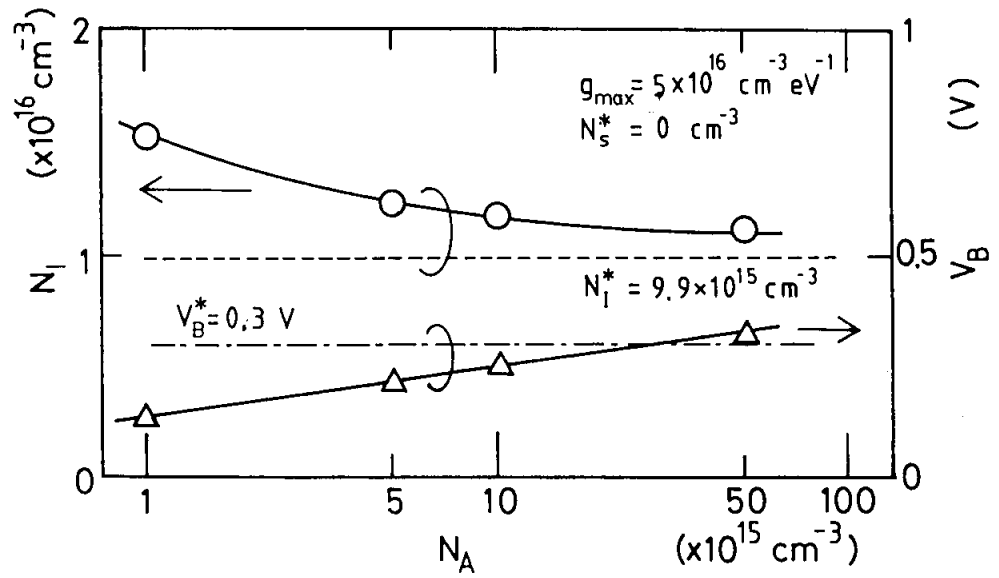

Fig.3.14. Dependencies of N_I and V_B obtained from steady-state HMC method on acceptor density in crystalline semiconductor without interface layer.

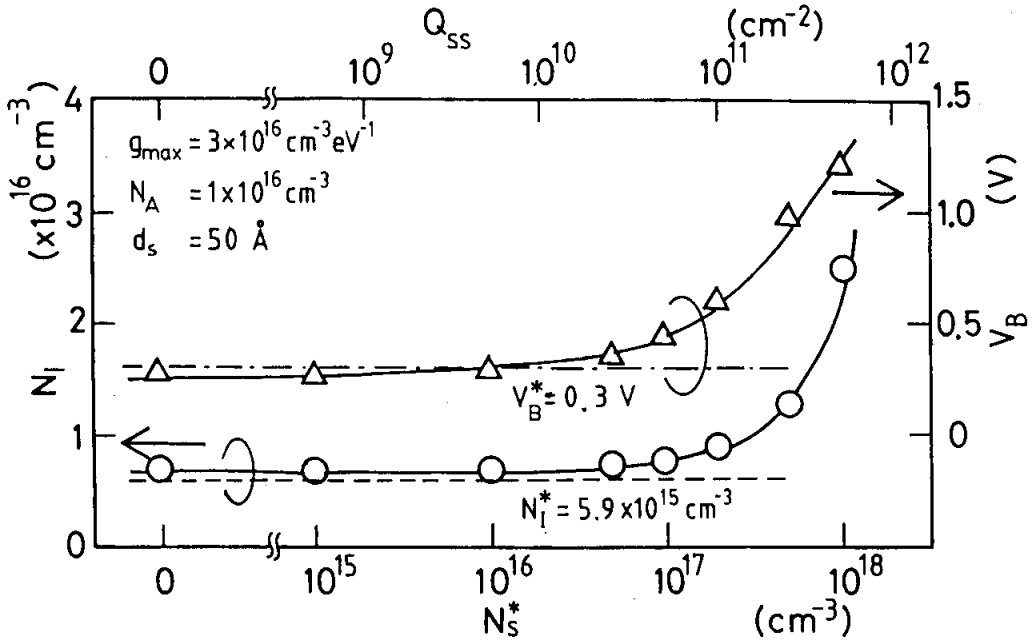

Fig.3.15. Dependencies of N_I and V_B on density of interface layer.

the interface layer was taken into account, were similar to those in Fig. 3.12, although the lowest reverse bias, where the discrepancy from the straight line starts to occur, is higher than the reverse bias (about 0.7 V) calculated without the effect of the interface layer. Figure 3.15 shows the dependence of N_I and V_B on the charge ($Q_{ss}=N_S^* d_s$) of the interface layer for $g_{max}=3\times10^{16}$ $cm^{-3}eV^{-1}$ and $N_A=10^{16}$ cm^{-3}. In the region of $N_S^* \leqq 2\times10^{17}$ cm^{-3} (i.e., the interface-state density Q_{ss} is less than 10^{11} cm^{-2}), the values of N_I and V_B are quite close to the values of N_I^* and V_B^*, respectively, then they increase rapidly with N_S^* in the case of $N_I^*=5.9\times10^{15}$ cm^{-3}. These increases result from Q_{ss}. This critical value of Q_{ss} (or N_S^*) increases with an increase of N_I^*.

It is clear from the above results that if Q_{ss} is low, the values of N_I and V_B obtained by the steady-state HMC method represent the real midgap-state density and the real built-in potential, respectively.

3-4. Summary

The high-frequency (e.g., 100-kHz) C-V characteristics of undoped (i.e., slightly n-type) a-Si:H/p c-Si heterojunctions have been studied experimentally as well as theoretically. These heterojunctions have been found to form depletion regions in both sides of a-Si:H and c-Si by dc bias voltages, and energy-band diagrams for those heterojunctions with four different resistivities of p c-Si have been presented. Since the measuring frequency is much higher than the reciprocal of the dielectric relaxation time of the high-resistivity undoped a-Si:H, the capacitance in the a-Si:H side is determined by the thickness of the a-Si:H film. That is why the measuring capacitance at the high frequency becomes a series of this capacitance in a-Si:H and the other capacitance which is determined by the width of the depletion region in c-Si. Moreover, the trapping/detrapping processes cannot respond to the high-frequency ac voltage, which easily enables us to analyze the C-V characteristics. The main